

# Structural basis of 5′ flap recognition and protein–protein interactions of human flap endonuclease 1

Hong Xu<sup>1,†</sup>, Rongyi Shi<sup>1,†</sup>, Wanchun Han<sup>1</sup>, Jiahui Cheng<sup>1</sup>, Xiaoli Xu<sup>1</sup>, Kaiying Cheng<sup>1</sup>, Liangyan Wang<sup>1</sup>, Bing Tian<sup>1</sup>, Li Zheng<sup>2</sup>, Binghui Shen<sup>1,2,\*</sup>, Yuejin Hua<sup>1,\*</sup> and Ye Zhao<sup>1,\*</sup>

<sup>1</sup>Key Laboratory of Chinese Ministry of Agriculture for Nuclear-Agricultural Sciences, Institute of Nuclear-Agricultural Sciences, Zhejiang University, Hangzhou, Zhejiang 310029, China and <sup>2</sup>Department of Cancer Genetics and Epigenetics, City of Hope National Medical Center and Beckman Research Institute, Duarte, CA 91010, USA

Received July 05, 2018; Revised September 20, 2018; Editorial Decision September 21, 2018; Accepted October 06, 2018

## ABSTRACT

**Human flap endonuclease 1 (hFEN1) is a structure-specific nuclease essential for DNA replication and repair processes. hFEN1 has 5′ flap removal activity, as well as gap endonuclease activity that is critical for restarting stalled replication forks. Here, we report the crystal structures of wild-type and mutant hFEN1 proteins in complex with DNA substrates, followed by mutagenesis studies that provide mechanistic insight into the protein–protein interactions of hFEN1. We found that in an  $\alpha$ -helix forming the helical gateway of hFEN1 recognizes the 5′ flap prior to its threading into the active site for cleavage. We also found that the  $\beta$ -pin region is rigidified into a short helix in R192F hFEN1–DNA structures, suppressing its gap endonuclease activity and cycle-dependent kinase interactions. Our findings suggest that a single mutation at the primary methylation site can alter the function of hFEN1 and provide insight into the role of the  $\beta$ -pin region in hFEN1 protein interactions that are essential for DNA replication and repair.**

## INTRODUCTION

Human flap endonuclease 1 (hFEN1) plays a key role in maintaining genomic stability by accurately processing DNA intermediates during replication and repair (1). Impaired DNA replication and repair due to hFEN1 deficiency is the underlying cause of many diseases including cancer (2). In addition to its flap endonuclease (FEN) activity, hFEN1 also exhibits relatively low levels of exonuclease (EXO) and gap endonuclease (GEN) activities (3).

The primary FEN activity of hFEN1, incising 5′ flaps at the single- and double-stranded DNA (ss-dsDNA) junction, is essential for Okazaki fragment maturation (4,5), long-patch base excision repair (6), and telomere leading-strand synthesis (7,8). The GEN activity of hFEN1, which potentially generates substrates for the recombination repair pathway, is important for processing stalled DNA replication forks (9,10).

Because nucleases digest DNA, FEN1 nuclease activity must be tightly controlled to ensure that it functions at the appropriate time and subcellular location. To date, at least three mechanisms have been proposed to regulate FEN1: precise substrate selection, protein–protein interactions and posttranslational modifications (PTMs). As a representative member of the 5′ structure-specific nuclease superfamily, FEN1 preferentially binds to sequence-independent double-flap DNA substrates, which contain both a 3′ and a 5′ flaps. The 1-nucleotide (nt) 3′ flap is first recognized by FEN1, leading to  $\sim 100^\circ$  bending of the DNA at the ss-dsDNA junction. Different models of 5′ flap recognition have been proposed. Recent biochemical and structural studies suggest that the inverted 5′ flap threads into the active site of hFEN1 via ‘phosphate steering’ guided by residues in its gateway and cap regions ( $\alpha 4$  and  $\alpha 5$ ) (11), which undergo a disorder-to-order transition upon substrate DNA binding.

FEN1 interacts with a number of proteins, including proliferating cell nuclear antigen (PCNA) (12,13), Werner syndrome helicase (WRN) (14,15), Rad9–Rad1–Hus1 (9–1–1) complex (16,17), and WDR4 (also known as WUHO) (18). These protein–protein interactions not only direct hFEN1 toward distinct DNA replication and repair substrates/pathways but also control the balance between its FEN and GEN activities. PCNA recruits FEN1 to the

\*To whom correspondence should be addressed. Tel: +86 571 86971279; Fax: +86 571 86971703; Email: yezhao@zju.edu.cn

Correspondence may also be addressed to Yuejin Hua. Email: yjhua@zju.edu.cn

Correspondence may also be addressed to Binghui Shen. Email: bshen@coh.org

<sup>†</sup>The authors wish it to be known that, in their opinion, the first two authors should be regarded as Joint First Authors.

DNA replication fork and stimulates FEN activity, which is critical for RNA primer removal (4). WRN stimulates both the FEN and GEN activities of FEN1 in coordination with PCNA (19). The 9–1–1 complex serves as a platform for DNA repair and enhances the FEN and GEN activities of FEN1 *in vitro* (20). More recently, it was demonstrated that WDR4 stimulates FEN activity and represses GEN activity (18).

hFEN1 undergoes multiple types of PTMs, including phosphorylation (21), methylation (22), acetylation (23,24), SUMOylation (25), ubiquitination (25) and succinylation (26). Of these PTMs, phosphorylation and methylation have been shown to antagonistically regulate hFEN1 activity (22). Phosphorylation of hFEN1 at Ser187 by cycle-dependent kinases reduces nuclease activity and PCNA binding and stimulates SUMOylation, ubiquitination, and proteasomal degradation (25). However, methylation of hFEN1 at Arg192 by the PRMT5 arginine methyltransferase strongly suppresses hFEN1 phosphorylation, which enhances interaction with PCNA (22).

Full length of hFEN1 has been co-crystallized with PCNA (13). Additional structural and biochemical analyses of FEN1 proteins have revealed elegant FEN1 regulatory mechanisms involving dsDNA bending, 3' flap recognition, 5' flap threading, and catalysis (27–33). However, the molecular basis for 5' flap capture prior to threading remains unclear. We report here the crystal structures of pre-threading and mutant (R192F) hFEN1–DNA complexes, which represent the complex before 5' flap binding and after methylation, respectively. These structures, together with mutagenesis and biochemical studies, provide mechanistic insights into 5' flap recognition by and the protein–protein interactions of hFEN1.

## MATERIALS AND METHODS

### Protein expression and purification

Full-length and C-terminally truncated hFEN1 (residues 1–380 and 1–333, respectively) were amplified by PCR and cloned into a modified pET28b expression vector, which contains a C-terminal 6× His-tag. Site-directed mutagenesis was performed with the QuickChange™ Site-Directed Mutagenesis Kit from Stratagene (La Jolla, CA, USA), as previously described (34). Primers used for cloning and mutagenesis are listed in Supplementary Table S1.

All hFEN1 proteins were expressed and purified as previously described (22). Briefly, transformed *Escherichia coli* strain BL21 (DE3) clones were grown at 37°C in LB medium containing 50 µg/ml Kanamycin to OD<sub>600</sub> of 0.6–0.8. Protein expression was induced by adding isopropyl-β-D-thioga-lactopyranoside (IPTG) to a final concentration of 0.4 mM at 16°C for 16 h. Cells were resuspended in lysis buffer (20 mM Tris (pH 7.8), 1 M NaCl, 5% glycerol, 3 mM β-ME, and 10 mM imidazole) after harvesting, lysed by sonication, and centrifuged at 18 000 × *g* for 45 min at 4°C. The supernatant was purified through a HisTrap HP column (GE Healthcare), equilibrated with buffer A (20 mM Tris [pH 7.8], 1 M NaCl, 5% [w/v] glycerol, and 10 mM imidazole), washed with 60 mM imidazole, and eluted with 300

mM imidazole. After desalting, the protein was loaded onto a HiTrap Q column (GE Healthcare) pre-equilibrated with buffer B (20 mM Tris [pH 7.8], 100 mM KCl, 5% [w/v] glycerol and 1 mM DTT). Fractions containing hFEN1 proteins were eluted with a linear gradient from 100 to 1000 mM KCl. The protein was finally purified through a Superdex 75 10/300 column (GE Healthcare) with buffer C (20 mM Tris [pH 7.8], 100 mM KCl, 0.1 mM EDTA, and 1 mM DTT) and stored at –80°C.

### Crystallization and structure determination

Crystallization was performed using the sitting drop vapor diffusion method at 293 K. Freshly purified C-terminally truncated hFEN1 at a concentration of ~15 mg/ml was centrifuged to remove the insoluble fraction before crystallization. The hFEN1–DNA binary complex was prepared by mixing hFEN1 and double-flap DNA at a 1:1.5 molar ratio and a concentration of ~5 mg/ml. After screening and optimization of the length and sequence context of double-flap DNA, crystals were grown in 35–40% (w/v) PEG 3350, 20 mM Tris (pH 7.8), 100 mM KCl and 10 mM MgCl<sub>2</sub>. Cryo-cooling was performed as previously described (35). Diffraction intensities were collected on the BL17U beamline at the Shanghai Synchrotron Radiation Facility (Shanghai, China) and were integrated and scaled using the X-ray Detector Software (XDS) suite (36). The structures were determined by molecular replacement using a published hFEN1 structure (PDB ID: 3Q8K) (30) as the search model. Structures were refined using PHENIX (37) and interspersed with manual model building using COOT (38). The refined models contained one hFEN1 in the asymmetric unit. The statistics for data collection and refinement are listed in Table 1. All residues are in the most favorable allowed regions of the Ramachandran plot. All structural figures were rendered in PyMol ([www.pymol.org](http://www.pymol.org)). The primer sequences used for crystallization are listed in Supplementary Table S1.

### Nuclease assays

Full-length hFEN1 proteins were used for nuclease assays. GEN activity and steady-state  $K_m$  and  $K_{cat}$  measurements were obtained using gapped and double-flap DNA substrates listed in Supplementary Table S1. All oligonucleotides were purchased from Sangon (Shanghai) with either 3'- or 5'-ends labeled with 6-carboxyfluorescein (6-FAM). For the GEN reaction, typically 1000–5000 nM hFEN1 were incubated with 1000 nM DNA in a 10 µl reaction volume containing 20 mM Tris (pH 7.5), 100 mM KCl, 5 mM NaCl<sub>2</sub>, 0.1 mg/ml BSA, 1 mM EDTA and 7 mM MgCl<sub>2</sub>. Reactions were carried out at 37°C for 30 min and terminated by the addition of formamide loading buffer (1 mM EDTA and 80% deionized formamide). After denaturation by heating at 95°C for 10 min, reaction products were resolved on 20% polyacrylamide sequencing gels containing 7 M urea. To measure the steady-state parameters, typically 0.05–16 nM hFEN1 was incubated with 25–1000 nM double-flap DNA for 10 minutes under the same conditions as the GEN reaction. All reactions were independently

**Table 1.** Statistics from crystallographic analysis

	Apo-protein Wild-type	Pre-threading D181A	Pre-threading D181A/R192F	Product R192F
<b>Data collection</b>				
Space group	<i>P</i> 2 <sub>1</sub> 2 <sub>1</sub> 2 <sub>1</sub>	<i>P</i> 2 <sub>1</sub> 2 <sub>1</sub> 2 <sub>1</sub>	<i>P</i> 2 <sub>1</sub> 2 <sub>1</sub> 2 <sub>1</sub>	<i>C</i> 222 <sub>1</sub>
Cell dimensions				
<i>a</i> , <i>b</i> , <i>c</i> (Å)	40.95, 61.07, 110.45	48.07, 93.83, 103.02	47.67, 92.73, 102.78	88.31, 244.76, 70.91
$\alpha$ , $\beta$ , $\gamma$ (°)	90, 90, 90	90, 90, 90	90, 90, 90	90, 90, 90
Resolution (Å)	30–1.90 (1.95–1.90)	30–1.95 (2.00–1.95)	30–2.25 (2.31–2.25)	30–2.3 (2.36–2.30)
<i>R</i> <sub>merge</sub>	9.3 (61.3)	3.3 (37.0)	9.1 (57.9)	7.1 (71.3)
<i>I</i> / $\sigma$ ( <i>I</i> )	13.8 (2.8)	23.7 (2.8)	11.1 (2.1)	16.1 (2.5)
Completeness (%)	99.9 (100.0)	98.0 (87.8)	98.8 (93.1)	98.8 (90.7)
Redundancy	5.9 (5.3)	4.6 (3.1)	5.7 (3.8)	5.1 (5.1)
<b>Refinement</b>				
Resolution (Å)	30–1.9	30–1.95	30–2.25	30–2.3
No. reflections	24041	33589	22086	34301
<i>R</i> <sub>work</sub> / <i>R</i> <sub>free</sub>	19.7/22.6	21.5/22.7	23.5/26.9	20.9/23.1
No. atoms				
Protein/DNA	2036/–	2290/806	2290/806	2483/791
Ion	6	1	1	–
Water	162	175	10	85
<i>B</i> factors				
Protein/DNA	29.25/–	44.05/57.50	52.54/67.83	55.76/88.93
Ion	46.67	128.80	133.83	–
Water	32.22	46.38	52.82	43.51
<b>RMSD</b>				
Bond length (Å)	0.005	0.005	0.009	0.008
Bond angle (°)	0.732	0.675	0.968	0.850
<b>Ramachandran statistics</b>				
Favored (%)	98.03	98.60	97.50	97.76
Allowed (%)	1.97	1.40	2.50	2.24
Outliers (%)	0	0	0	0

Values in parentheses refer to the highest resolution shell.

$R_{\text{factor}} = \sum |F(\text{obs}) - F(\text{calc})| / \sum F(\text{obs})$ .

$R_{\text{free}} = R$  factor calculated using 5.0% of the reflection data randomly chosen and omitted from the start of refinement.

RMSD = root-mean-square deviation.

repeated at least six times. Quantification and curve fitting were carried out as previously described (29,39).

### Cell culture and western blot analysis

To isolate HeLa cell lines stably-expressing hFEN1 proteins, cells were cultured in DMEM supplemented with 10% FBS and were transfected with pEZ-M12-ef1 $\alpha$ -3  $\times$  Flag plasmids containing full-length wild-type, K200A, K201A, K200/201A or R192F hFEN1. Stable cell lines were established by G418 selection and verified by immunofluorescence staining with an anti-FLAG antibody. About 4  $\times$  10<sup>6</sup> cells were collected and lysed with RIPA Lysis Buffer (Beyotime, CH) containing a protease inhibitor cocktail (Roche, CH). Whole-cell extracts were subjected to immunoprecipitation with anti-FLAG M2 magnetic beads (Sigma, USA), and cell extracts or immunoprecipitates were resolved by SDS-PAGE followed by electrotransfer onto PVDF membranes and incubation with primary (1:1000 dilution, Abcam, GB) and secondary (1:2000 dilution, Ptg lab, USA) antibodies sequentially after blocking. The membranes were further washed with TBST and developed using ECL reagents (Pierce, MA, USA).

### Cell cycle synchronization

HeLa cell lines were synchronized in mid S phase using a double-thymidine block method in which cells were treated

with 2.5 mM thymidine (Sigma, USA) for 15 h, released for 8 h in thymidine-free medium, and treated with 2.5 mM thymidine again for another 18 h, followed by 3 h of release in thymidine-free medium before cell collection.

## RESULTS

### Overall structure and catalytic center configuration of hFEN1 nuclease

To investigate the mechanisms by which hFEN1 is regulated, we generated wild-type, D181A, R192F, and D181A/R192F mutant hFEN1 proteins for co-crystallization with a double-flap DNA substrate. It is known that the C-terminus of FEN1 is structurally disordered, which makes crystallization difficult. Therefore, for crystallization, we used C-terminally truncated wild-type and mutant hFEN1 (residues 1–333; Supplementary Figure S1), which contain the entire catalytic site and are expected to be fully competent for catalysis (20,30). We chose to investigate the D181A mutation because among mutations to conserved amino acids in FEN1, it was found to reduce hFEN1 cleavage activity to the greatest extent (40). Our previous study (22) and studies by other groups (41,42) have demonstrated that substitution of arginine residues with phenylalanine residues can mimic arginine methylation for biochemical characterization. Therefore, we replaced the primary methylation site Arg192 of hFEN1

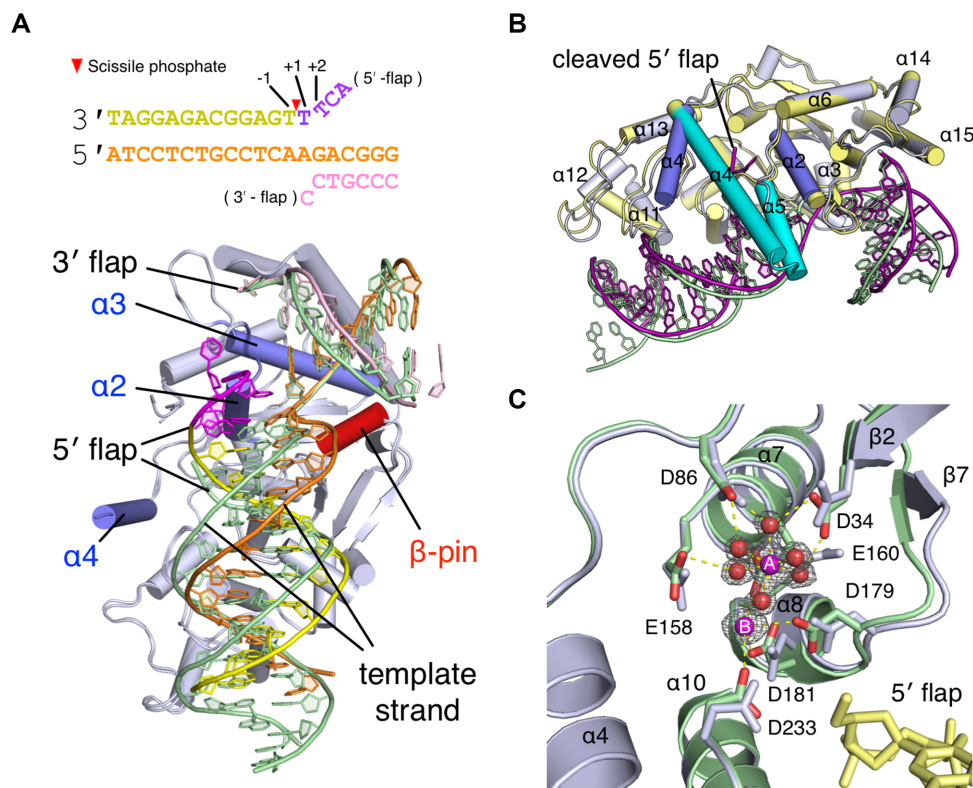


**Figure 1.** Overall structural comparison of the hFEN1 nuclease core domain. (A) Superposition of D181A/R192F and R192F hFEN1–DNA structures. A schematic of the DNA substrate used for crystallization is shown on top with colors corresponding to those in the structures below. The hFEN1 protein is colored in white with gateway and cap helices ( $\alpha 2$ ,  $\alpha 3$  and  $\alpha 4$ ) labeled and shown in blue. The  $\beta$ -pin region is colored red. The DNA template strand in the D181A/R192F hFEN1–DNA (pre-threading) structure is drawn in orange with the 3' and 5' flap strands in pink and yellow, respectively. The part of the 5' flap to be cleaved in the product structure is in magenta. The DNA in the R192F hFEN1–DNA (product) structure is drawn in green. (B) Superposition of two hFEN1 product complexes. The hFEN1–DNA product structure solved in the current study has the same coloring as in A. The published hFEN1 product structure (PDB ID: 3Q8K) is colored in yellow with DNA in magenta and cap helices  $\alpha 4$  and  $\alpha 5$  in cyan. (C) Superposition of the active site of the hFEN1 apo-protein structure (green) and product structure (white). The catalytic residues and 5' flap end (yellow) are labeled and shown as sticks. Two metal ions (A and B) and six coordinating water molecules (red) in the apo-protein structure are shown as spheres.

with phenylalanine. Although phenylalanine does not perfectly mimic methylation of the arginine residue, both methylation and substitution with phenylalanine increase protein hydrophobicity. Furthermore, we found previously that R192F hFEN1 has a phosphorylation pattern and PCNA binding activity similar to those of methylated hFEN1 *in vitro* and in cells (22). The crystals were grown in the presence of  $Mg^{2+}$  ions and diffracted X-rays to 1.9–2.3 Å resolution (Table 1). Wild-type hFEN1 was crystallized in the apo-form, and the structures of two types of hFEN1–DNA complexes were obtained (Figure 1A and Supplementary Figure S2). The intact 5' flap was observed in both the D181A and D181A/R192F hFEN1–DNA structures in which the –1 and +1 bases (relative to the 5' and 3' side of the scissile phosphate) remained base-paired with the DNA template strand (Figure 1A and Supplementary Figure S2B, C). Therefore, we consider these to be ‘pre-threading’ structures. In the R192F hFEN1–DNA structure, which represents the cleaved product complex, the 5' flap strand was cleaved but not engaged with the active site (Figure 1A, B and Supplementary Figure S2D).

The overall conformation of these hFEN1 structures can be virtually superimposed onto the previously solved hFEN1 threading structure (Protein Data Bank [PDB] ID:

5UM9). The gateway and cap helices  $\alpha 2$ ,  $\alpha 4$  and  $\alpha 5$  are completely disordered in the hFEN1 apo-protein structure (Supplementary Figure S2A). In all three hFEN1–DNA structures, however, the  $\alpha 2$  helix becomes ordered upon interaction with the substrate DNA, which induces the DNA duplex to bend sharply at approximately  $100^\circ$  (Figure 1A, B and Supplementary Figure S2B–D). We also observed that the partially structured  $\alpha 4$  helix in the R192F hFEN1–DNA product complex is shifted away from the active site compared to that in the published product structure (PDB ID: 3Q8K; Figure 1B and Supplementary Figure S2D). However, the cap region (part of the  $\alpha 4$  and  $\alpha 5$  helices; Supplementary Figure S1) is disordered in all four structures solved in this study (Supplementary Figure S2B–D). These observations are consistent with the disorder-to-order transition of hFEN1 upon dsDNA binding.

Despite their nearly identical protein conformations, only the active site of the hFEN1 apo-protein structure but not of the hFEN1–DNA structures contained an electron density corresponding to the catalytic metal ions, which were positioned 4 Å apart (Figure 1C and Supplementary Figure S2A). These two metal ions are coordinated by seven conserved acidic hFEN1 residues and water molecules (Figure 1C and Supplementary Figure S1). The A site metal ion,

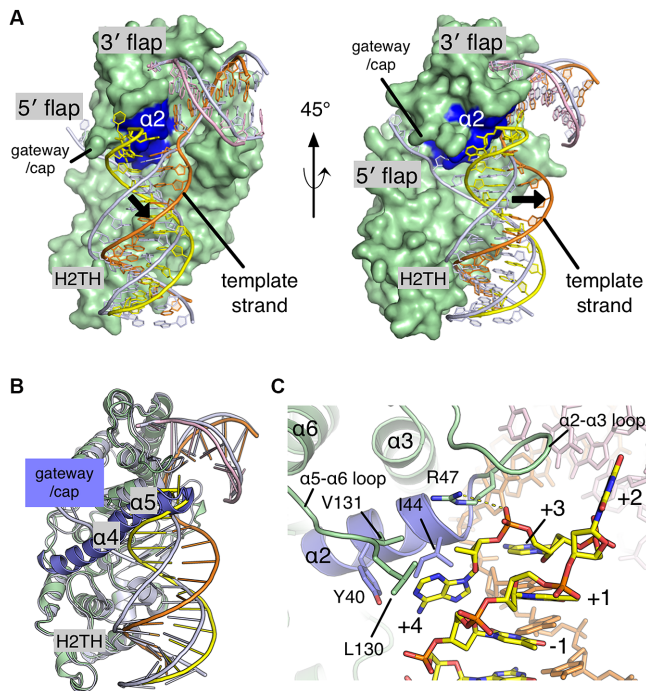


**Figure 2.** Pre-threading structure of the hFEN1–DNA complex. (A) Superposition of double-flap DNA in the hFEN1 pre-threading structure (colored) and the published threading structure (white, PDB ID: 5UM9). The protein is represented by the green surface, and the  $\alpha 2$  helix is shown in blue. The template strand, 5' flap, 3' flap, gateway/cap, and H2TH binding site are labeled. The black arrowhead indicates the DNA shift between the threading and pre-threading structures. (B) Superposition of the hFEN1 pre-threading structure (green) and threading structure (white, PDB ID: 5UM9). The unthreaded 5' flap in the pre-threading structure is colored yellow. The gateway and cap helices ( $\alpha 4$  and  $\alpha 5$ ) in the threading structure are in blue. (C) Interactions between hFEN1 and the unthreaded 5' flap in the D181A hFEN1–DNA pre-threading structure. Helices, loops, and nucleotide bases of the 5' flap are labeled. Protein side chains involved in the protein–5' flap interactions are shown as sticks.

in its hexa-aquated form, is coordinated by Asp34, Asp86, Glu158 and Glu160, whereas the B site metal ion is coordinated by Asp179, Asp181 and Asp 233. The overall configuration and these catalytic residues align well with that of hFEN1 in complex with the inhibitor *N*-hydroxyurea (PDB ID: 5FV7; Supplementary Figure S3). Compared to that in the hFEN1 product structure,  $\beta 7$  in the hFEN1 apo-protein structure is shifted toward the active site, and Glu160 undergoes substantial rotamer change upon metal coordination (Figure 1C).

### Pre-threading hFEN1–DNA complexes: substrate interactions and functional implications

hFEN1 and the upstream DNA containing the 3' flap could be adequately superimposed in all the hFEN1–DNA structures (Figure 1A). However, the downstream DNA in both the D181A and D181A/R192F hFEN1–DNA structures is shifted away from the active site compared with that in the published threading structure, which contains a 5' flap threaded through the helical gateway/cap (PDB ID: 5UM9; Figure 2A, B). Clear electron density of the unthreaded 5' flap was observed in the D181A and D181A/R192F

hFEN1–DNA structures, because it lies outside the active site, occupying nearly the same space as the  $\alpha 5$  helix observed in the hFEN1 threading structure (Figure 2B and Supplementary Figure S4A). The distance between the scissile phosphate and the active site divalent metals is  $>16$  Å in these two structures.

The downstream dsDNA in our pre-threading structures is anchored to the helix-2turn-helix (H2TH) motif, as observed in all the hFEN1–DNA structures (Figure 2A, B). The  $\alpha 2$  helix and two loops ( $\alpha 2$ – $\alpha 3$  and  $\alpha 5$ – $\alpha 6$ ) interact with the unthreaded 5' flap through hydrogen bonds, stacking interactions, and van der Waals interactions (Figure 2C and Supplementary Figure S4A, B). As noted above, in the hFEN1 pre-threading structures, the +1 and –1 bases of the 5' flap remain base-paired. The +2 base makes contact with the  $\alpha 2$ – $\alpha 3$  loop, and the +3 base is inserted between the +1 base-pair and the  $\alpha 2$  helix. Arg47 at the end of the  $\alpha 2$  helix interacts with the +3 nucleoside, and the +4 base is held in place by four side chain residues: Tyr40, Ile44, Leu130 and Val131.

Two residues, Tyr40 and Arg47, have been reported to play multiple roles in hFEN1 cleavage (11,30). Tyr40, at the entrance of the active site, stabilizes the ordered helical gateway and packs against either the +1 or –1 base during cleavage (Supplementary Figure S4b,c). In the pre-threading structures, Tyr40 adopts a rotamer conformation similar to that in the published hFEN1–DNA product complex (PDB ID: 5K97; Supplementary Figure S4b). Arg47, on the other side, forms a salt bridge with the phosphate group and a stacking interaction with the sugar pucker of the +3 nucleoside (Figure 2c and Supplementary Figure S4b). To further confirm the interactions between Arg47 and the 5' flap, we replaced Arg47 with lysine, which has an amino group that mimics the electrostatic interaction and hydrogen-bonding ability of Arg but has substantially reduced stacking interaction potential. We measured the  $K_m$  and  $K_{cat}$  of double-flap DNA cleavage by the R47K mutant hFEN1. The  $K_m$  of R47K was 4-fold greater than that of wild-type hFEN1, and the  $K_{cat}$  was approximately 8-fold lower than that of the wild-type hFEN1, resulting in 30-fold lower overall efficiency ( $K_{cat}/K_m$ ; Supplementary Table S2).

### Loop-to-helix transition of the $\beta$ -pin region that potentiates the FEN activity for RNA primer removal

Bending of the duplex DNA at the ss-dsDNA junction is an essential event prior to 5' flap threading by hFEN1. In addition to the helical gateway and cap helices, the  $\beta$ -pin region between  $\beta 8$  and  $\beta 9$  (residues 194–200, LTASEAK) interacts with the dsDNA at the bending point, as previously observed (Figure 1A and Supplementary Figure S2) (30). In the wild-type and D181A hFEN1–DNA structures, the  $\beta$ -pin region adopts a loop conformation, as observed in all crystallized hFEN1 to date (Supplementary Figures S2a, b and S5a). Unexpectedly, this  $\beta$ -pin region is rigidified into a short helix in both D181A/R192F and R192F hFEN1–DNA structures, which contain a point mutation at the primary methylation site of hFEN1 (Figure 3A and Supplementary Figure S2C, D). However, this conformational change does not alter the position of  $\beta 8$  and  $\beta 9$  in

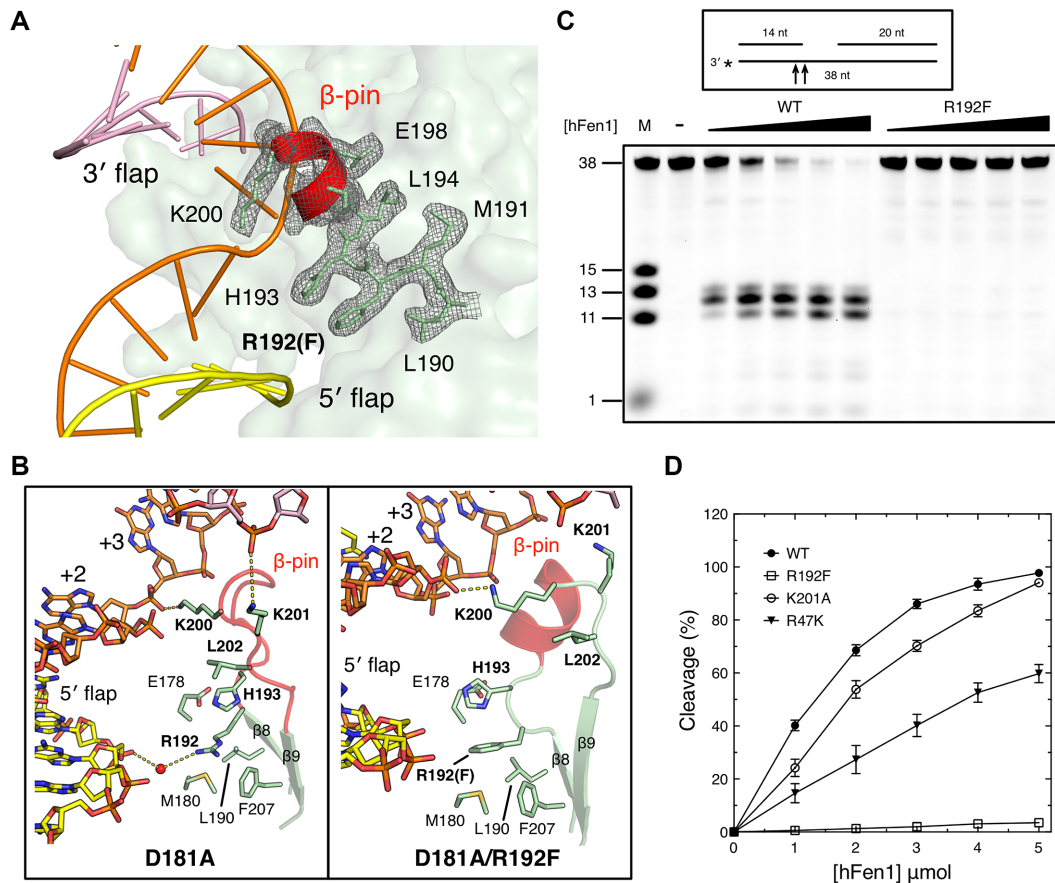


**Figure 3.** Loop-to-helix transition of the  $\beta$ -pin region in the R192F hFEN1–DNA structure. (A) The electron densities of phenylalanine at the 192 position and of the  $\beta$ -pin helix are shown in grey with the refined 2Fo–Fc map contoured at  $1\sigma$ . (B) Interactions between the  $\beta$ -pin and DNA in D181A (left) and D181A/R192F (right) hFEN1–DNA structures. The  $\beta$ -pin region adopting a loop or helix conformation is colored red. The yellow dashed lines indicate interactions between lysine residues and DNA through a water molecule (red sphere). (C) Denaturing PAGE gel showing reduced GEN activity of the R192F mutant compared to wild-type (WT) hFEN1. 3'-fluorescence-labeled gapped DNA (1  $\mu$ M) was incubated with 1, 2, 3, 4 or 5  $\mu$ M of R192F or WT hFEN1 proteins in the presence of  $Mg^{2+}$ . M indicates the DNA markers. (D) Quantification of GEN product cleavage by WT and mutant hFEN1 proteins.

any of the hFEN1 structures solved in this study (Supplementary Figure S5B).

The transition from the loop conformation to the helix conformation was only observed when arginine was replaced by phenylalanine. Why is this so? In the pre-threading D181A hFEN1–DNA structure, Arg192 (located at the end of  $\beta 8$ ) interacts with the  $-3$  phosphate group through a water molecule (Figure 3b, left panel). Moreover, Arg192 is surrounded by three nonpolar residues (Met180, Leu190, and Phe207) and forms an aromatic  $\pi$ -interaction with His193. Phenylalanine substitution of arginine increases hydrophobicity at the 192 position, favoring the loop-to-helix transition. Indeed, in both the R192F and D181A/R192F hFEN1–DNA structures, His193 shows clear movement toward the DNA minor groove due to the favorable aromatic interactions between the phenylalanine and surrounding residues (Figure 3B and Supplementary Figure S5C), which further stabilize the helical conformation of the  $\beta$ -pin region. Leu202, however, shifts  $>4$  Å in the opposite direction because its interaction with His193 is lost (Supplementary Figure S5C).

Steady-state kinetic parameters were measured using full-length hFEN1 to complement our structural observation of the  $\beta$ -pin helix formation. Three residues, Arg192, Lys200 and Lys201, were mutated based on the D181A/R192F hFEN1–DNA structure (Figure 3B). The R192F mutant exhibited approximately 5-fold lower FEN activity relative to wild-type hFEN1 (Supplementary Table S2), which was consistent with the interaction between Arg192 and downstream dsDNA (Figure 3B). Surprisingly, the GEN activity of the R192F mutant was almost eliminated, resulting in only a 1-nt EXO product at high hFEN1 concentrations (Figure 3C, D and Supplementary Figure S6). Kinetic analysis revealed that the  $K_{cat}/K_m$  for the GEN activity of WT FEN1 was  $0.015 \mu M^{-1} min^{-1}$  (Supplementary Table S2). However, we could not determine the  $K_{cat}/K_m$  of R192F because the GEN product of R192F was not detected. Thus, the R192F mutation appears to favor the FEN activity of hFEN1 over its GEN activity. In the D181A hFEN1–DNA structure, two positively charged residues located at the end of the  $\beta$ -pin, Lys200 and Lys201, interact with the  $+3$  phosphate group of the template strand and upstream DNA, respectively (Figure

3B). In the D181A/R192F hFEN1–DNA structure, a salt bridge between Lys200 and the +2 position phosphate of the template strand is maintained. Therefore, alanine substitution of Lys200 impaired the FEN and GEN activity of hFEN1 by 125- and 8-fold (Supplementary Table S2). Lys201, however, shifts away from the upstream DNA in the D181A/R192F hFEN1–DNA structure, and their interaction is lost (Figure 3B, right panel). Thus, replacing Lys201 with alanine had little effect on its FEN and GEN activities (Figure 3C, D and Supplementary Table S2).

### The $\beta$ -pin region is a key motif involved in protein/protein interactions that direct FEN1 toward DNA replication or repair pathways

Because the  $\beta$ -pin region is solvent-exposed in the hFEN1 apo-protein structure, we suspected that it might be involved in protein–protein interactions. The interactions between hFEN1 and partner proteins are essential to ensure precise and accurate incision at the correct location. The antiparallel  $\beta$ - $\beta$  interactions between hFEN1 and PCNA were observed in the previously solved hFEN1–PCNA structure (13). In addition, several residues in the hFEN1 core domain ( $\beta$ 1 and  $\eta$ 2; Supplementary Figure S1) interact directly with the PCNA molecule. To further investigate the hFEN1–PCNA interactions, we modeled the interaction between methylated hFEN1 and PCNA based on the superposition of our D181A/R192F hFEN1–DNA structure and the published hFEN1–PCNA complex (PDB ID: 1UL1; Figure 4A). According to our model, the helical  $\beta$ -pin is located next to the  $\eta$ 2 helix, which is a key element at the interface between hFEN1 and PCNA. Thus, the transition of the  $\beta$ -pin loop into a helix might constrain the protein–protein interface, facilitating hFEN1–PCNA binding.

To further examine hFEN1 protein–protein interactions, we established stable cell lines individually expressing full-length 3 $\times$  Flag-tagged wild-type, R192F, K200A, K201A and K200/K201A hFEN1s and performed co-immunoprecipitation assays (Figure 4B, C and Supplementary Figure S7). As expected, R192F hFEN1 exhibited less than 25% phosphorylation and slightly but significantly enhanced PCNA binding affinity compared to the wild-type protein (Figure 4B). Interactions with CDK2 and Cyclin E were also 40% and 70% lower, respectively, for R192F versus wild-type hFEN1. The CDK2/Cyclin E complex catalyzes FEN1 S187 phosphorylation. Therefore, reduced hFEN1 phosphorylation is likely due to impaired interactions with these kinases. (Figure 4B). Consistent with this supposition, alanine substitution of Lys200 and Lys201 reduced both CDK2 and Cyclin E binding to various degrees, which in turn diminished hFEN1 phosphorylation (Figure 4C). In addition to moderately decreased PCNA interactions, K200A and K201A mutants both lost the ability to bind Rad1 by  $\sim$ 40% compared to wild-type. The K200A mutant had  $\sim$ 60% lower hFEN1–WDR4 interactions compared to wild-type, whereas the K201A mutant showed enhanced WDR4 binding affinity. These results are consistent with *in vitro* analyses of the interactions of purified His-tagged hFEN1 proteins with proteins in HeLa cell lysates (Supplementary Figure S8).

## DISCUSSION

hFEN1 is an essential nuclease that maintains genome stability and plays a critical role in DNA replication and repair. Defects in hFEN1 that compromise its protein function are unequivocally associated with cancer (6,43). Because FEN1 is a structure-specific nuclease, proper 5' flap DNA binding is key for accurate cleavage. Previous studies show that despite little overall structural change, the gateway and cap ( $\alpha$ 2,  $\alpha$ 4 and  $\alpha$ 5) regions of hFEN1 undergo disorder-to-order transitions upon substrate DNA binding (11,28,30). In this study, we found that these helices are completely disordered in the DNA-free hFEN1 protein (Supplementary Figure S2). The ordered  $\alpha$ 2 helix is bound to the 3' flap in both pre-threading structures of hFEN1. The  $\alpha$ 4 helix becomes partially structured, but the cap region, including the  $\alpha$ 5 helix, remains disordered in the hFEN1 product complex. Notably, the cap region is ordered in all published structures of hFEN1 threading and product complexes containing catalytic metals in the active site (11,30). However, no metal ion could be located in the active site of our hFEN1 product complex, indicating that a well-formed active site containing catalytic metals may be required for the disorder-to-order transition of the cap region. Furthermore, two  $Mg^{2+}$  ions, which have been proposed to be critical for interactions between FEN1 and its inhibitor *N*-hydroxyurea (44), were observed in the active site of the hFEN1 apo-protein structure (Figure 1C). Binding of the inhibitor was found to disturb the active site formation by not only changing the position of the metals but also increasing the distance between the two  $Mg^{2+}$  ions relative to their positions in the apo-protein structure (Supplementary Figure S3). Thus, we consider it plausible that inhibitor binding could destabilize the active site and preclude the disorder-to-order transition of the cap region, further suppressing cleavage.

The intact 5' flap was directed away from the active site in both pre-threading structures, which represent the hFEN1–DNA complex before 5' flap binding (Figure 2A). Like other structure-specific nucleases, hFEN1 must meet several conditions prior to cleavage to ensure the specific incision of the flapped DNA substrate. In contrast to other endonucleases that form continuous DNA-binding surfaces, hFEN1 interacts with DNA mainly at the downstream dsDNA and the active site, resulting in severe DNA bending. Despite the shifted DNA after bending, these two DNA-binding sites remain in the pre-threading structures (Figure 2A and B), which is consistent with the proposed 'measure twice, cut once' mechanism (45). Several models for 5' flap recognition by FENs have been proposed, and threaded 5' flaps have been observed in both hFEN1- and T5FEN-DNA structures (11,46). In our pre-threading structures, both the +1 and –1 bases of the 5' flap remain base-paired to the template strand (Figure 2C). The unthreaded 5' flap is engaged by the  $\alpha$ 2 helix and by the loop region before the  $\alpha$ 6 helix. Two residues, Tyr40 and Arg47, are important for arranging the gateway and form multiple interactions with the 5'-flap nucleotides. Overall nuclease activity of R47K mutant hFEN1 is greatly reduced, partly due to its reduced ability to form a cation- $\pi$  stack with the 5' nucleotide. Considering previous observations of the base-paired dsDNA in the

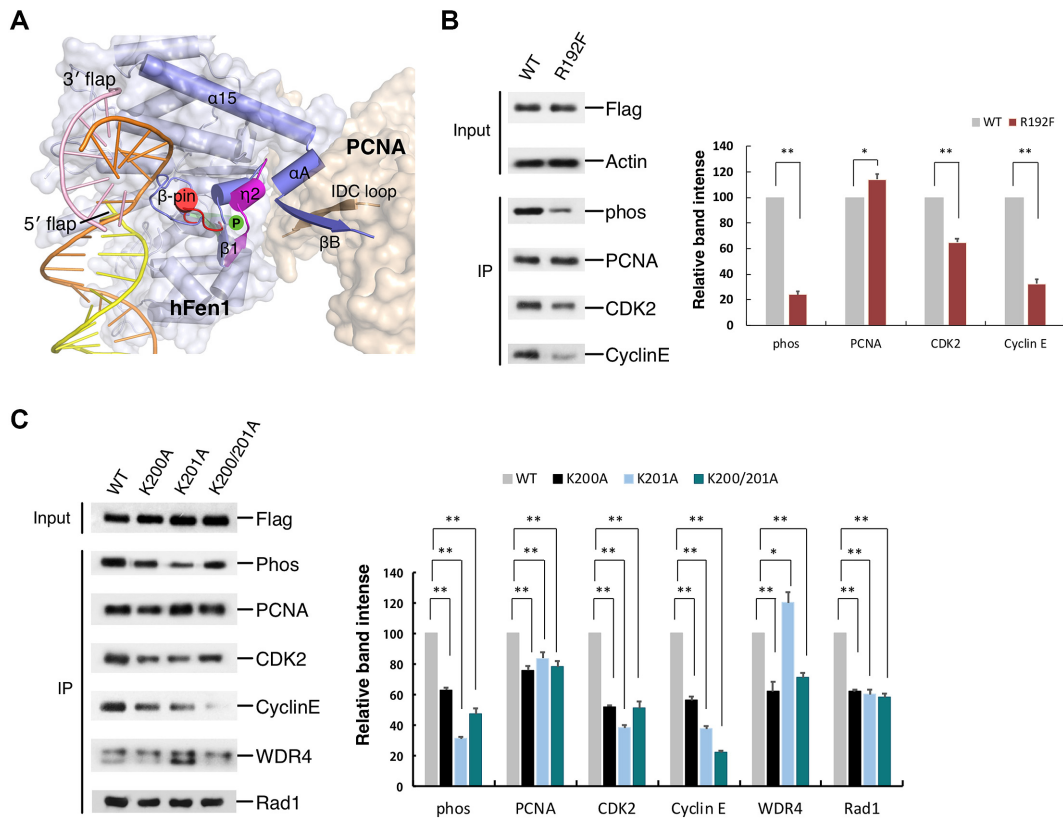


**Figure 4.** Interactions between hFEN1 and partner proteins. (A) Methylated hFEN1–PCNA model. hFEN1 and PCNA in the published hFEN1–PCNA structure (PDB ID: 1UL1) are shown in blue and wheat, respectively. The helices and  $\beta$ -sheets located at the R192F hFEN1–PCNA interface are also illustrated. The  $\beta$ -pin region is shown in red, and  $\beta$ 1 and the  $\eta$ 2 helix are in magenta. The position of the hFEN1 phosphorylation site (Ser197) is indicated in green. (B) Comparison of the protein interaction abilities of R192F and wild-type (WT) hFEN1. M2-beads were incubated with cell lysate to immunoprecipitate hFEN1 with its complex. The phosphorylation level of hFEN1 and its binding ability with the indicated proteins was evaluated by western blot analysis. (C) Cellular effects of alanine mutations at two  $\beta$ -pin residues of hFEN1. Immunoprecipitation and western blot analysis were conducted, as described for panel (B). Values are means  $\pm$  S.D. of three independent assays. *P* values (\* $<$ 0.05, \*\* $<$ 0.01) were calculated using Student's *t*-tests.

active site of hFEN1 (11), our pre-threading structures suggest that the helical gateway, in addition to the cap helices, is also involved in 5' flap recognition and the orientation of dsDNA into the active site.

Methylation of arginine side chains increases regional hydrophobicity (47). hFEN1 is symmetrically di-methylated at Arg192 and is recruited to the replication fork by PCNA in early S phase (22). hFEN1 methylation strongly inhibits its subsequent phosphorylation. Therefore, after cleavage, hFEN1 is demethylated prior to phosphorylation, which results in reduced FEN activity and dissociation from PCNA. To explore the possible molecular mechanisms by which methylation regulates hFEN1, we determined the crystal structures of R192F and D181A/R192F hFEN1 in complex with DNA. Although phenylalanine does not perfectly mimic the methylation of arginine, it increases hydrophobicity at the primary methylation site and has been used for studying the effects of arginine methylation by our and other groups (22,41,42). In both hFEN1–DNA structures, the  $\beta$ -pin region connecting  $\beta$ 8 and  $\beta$ 9 undergoes a loop-to-helix transition (Figure 3A), rendering these structures distinctly different from all other hFEN1 structures solved to

date. The  $\beta$ -pin helix formation enhances interactions with surrounding hydrophobic residues, especially the aromatic His193 (Supplementary Figure S5c). Enhanced hydrophobic interactions due to arginine methylation have also been observed in the human histone/chromodomain structure (48) and the  $\beta$ -hairpin model system (49). Symmetrically di-methylated Arg192 was also modeled in our hFEN1–DNA structure (Supplementary Figure S9). The methylated arginine appears to be able to maintain hydrophobic interactions with surrounding residues, similarly to phenylalanine, with no obvious steric clash.

We proposed the following hFEN1 regulation mechanisms based on our hFEN1–DNA structures and *in vitro* biochemical studies. First, methylation at the Arg192 site might induce the conformational change of the  $\beta$ -pin region, which makes it more rigid. The  $\beta$ -pin maintains interactions with the upstream dsDNA (Figure 3B), and the FEN activity of hFEN1 is only slightly attenuated. However, this  $\beta$ -pin conformation could orient the  $\eta$ 2 helix and residues at the hFEN1–PCNA interface (Figure 4A) to enhance recruitment to the DNA replication fork. Furthermore, our mutagenesis studies suggest that the  $\beta$ -pin re-

gion of the nuclease core is also involved in the direct protein–protein interactions of hFEN1. Alanine substitutions of two  $\beta$ -pin residues, Lys200 and Lys201, weakened the interactions of hFEN1 with WDR4 and Rad1, as well as with the protein kinases (Figure 4C). Moreover, these mutations could also destabilize the hFEN1–PCNA interface, leading to reduced PCNA binding. Second, after cleavage and JMJD1B-mediated demethylation, hFEN1 is typically phosphorylated (50). The phosphorylation site Ser187, however, is located close to the hFEN1–PCNA interface (Figure 4A). Therefore, the binding of PCNA, enhanced by hFEN1 methylation, may partially block the access of protein kinases to the phosphorylation site, which is consistent with the impaired interactions between R192F and the protein kinases CDK2 and Cyclin E, as well as the reduced phosphorylation level of R192F *in vivo* (Figure 4B). Third, in addition to its well-known FEN activity, hFEN1 possesses GEN and EXO activities. These distinct nuclease activities target different types of DNA substrates and must be tightly controlled. We observed that the R192F hFEN1 was defective for GEN activity but retained FEN activity (Figure 3C). These observations were reminiscent of the action of the E160D mutation in FEN1 (43). E160D selectively eliminates the GEN and EXO activities of FEN1, and heterozygous E160D mutation in mice results in the initiation and progression of cancers. In addition, WDR4 interactions with the FEN1/PCNA complex also suppress the GEN activity and promote the FEN activity for flap removal at the unstressed replication fork to maintain genome stability (18). Thus, methylation, as well as protein–protein interactions, might also control the balance between the FEN and GEN activities of hFEN1 to ensure accuracy during DNA replication.

We also observed that the cleavage of the GEN substrate by hFEN1 was less efficient than that of the FEN substrate (Supplementary Table S2), which is probably due to the lack of a free 5' flap. Although the detailed mechanisms of GEN cleavage by hFEN1 are poorly understood, the ssDNA region of gapped DNA is thought to roll into the active site for cleavage. In our pre-threading structures, the  $\alpha$ 2 helix contacts the ssDNA portion of the free 5' end, and the R47K mutant protein with reduced 5' interactions exhibited impaired GEN activity (Figure 3D and Supplementary Table S2). These findings indicate that this protein–DNA interface is another important regulator of hFEN1 GEN cleavage.

Collectively, our results unveil several mechanisms by which hFEN1 activity is regulated (Figure 5). Methylation at the Arg192 site during DNA replication possibly induces the conformational change of the  $\beta$ -pin region of hFEN1 and enhances its PCNA binding and loading onto the DNA replication fork. During DNA replication, GEN activity of hFEN1 is suppressed by both methylation and partner proteins. For example, interaction with WDR4 ensures FEN activity for flap removal. Demethylation after cleavage is an essential step prior to phosphorylation, as both methylation and PCNA binding impair the interactions between hFEN1 and protein kinases. Additionally, the  $\beta$ -pin region in the nuclease core of hFEN1 participates in the recruitment of hFEN1 in response to DNA damage, which promotes both FEN and GEN activities.

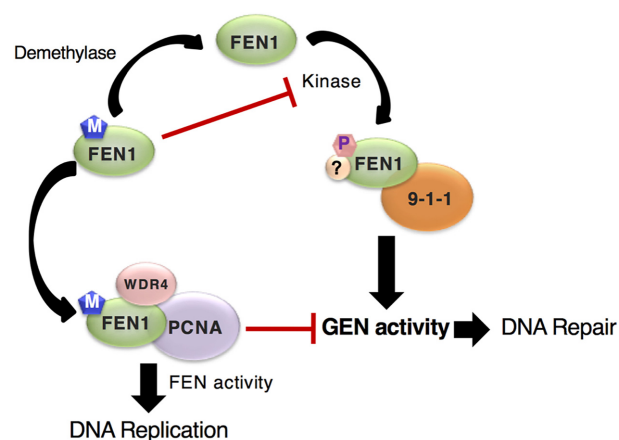


**Figure 5.** A model of methylation-based regulation of hFEN1. Upon methylation at the Arg192 site, the  $\beta$ -pin loop of hFEN1 is rigidified into a short helix. The loop-to-helix transition of the  $\beta$ -pin region ensures hFEN1 interactions with PCNA and WDR4 to remove the flapped DNA substrate. At this time both GEN activity and protein kinases interactions are suppressed. After demethylation, hFEN1 undergoes phosphorylation and possibly other types of posttranslational modifications. During DNA repair, the GEN activity of hFEN1 is stimulated by interactions with DNA repair proteins (e.g. the 9–1–1 complex).

## DATA AVAILABILITY

The coordinates and structure factors have been deposited to the Protein Data Bank with accession codes 5ZOD (wild-type apo-protein structure), 5ZOE (D181A hFEN1–DNA structure), 5ZOG (R192F hFEN1–DNA structure), and 5ZOF (D181A/R192F hFEN1–DNA structure).

## SUPPLEMENTARY DATA

Supplementary Data are available at NAR Online.

## ACKNOWLEDGEMENTS

We would like to thank the staff at the Shanghai Synchrotron Radiation Facility (SSRF; China) for assistance in data collection. We thank Dr. Kerin at City of Hope for editorial assistance of the manuscript.

*Author contributions:* Y.Z., Y.H. and B.S. conceived the project. H.X., R.S., X.X. and L.Z. designed and carried out co-immunoprecipitation assays. R.S. and J.C. carried out mutagenesis, biochemical experiments, and kinetics analyses. W.H. and J.C. purified proteins and carried out crystallization and data collection. H.X., L.Z., B.S., Y.H., B.S. and Y.Z. contribute to the manuscript preparation. All authors discussed the results and commented on the manuscript.

## FUNDING

National Basic Research Program of China [2015CB910600]; National Key R&D Program of China [2017YFA0503900]; Zhejiang Provincial Natural Science Foundation for Outstanding Young Scientists [LR16C050002]; National Natural Science Foundation of China [31210103904, 31500656, 31670819]; National Institutes of Health [R01CA073764 and R50CA211397].

*Conflict of interest statement.* None declared.

## REFERENCES

- Dehe, P.M. and Gaillard, P.H. (2017) Control of structure-specific endonucleases to maintain genome stability. *Nat. Rev. Mol. Cell Biol.*, **18**, 315–330.
- Balakrishnan, L. and Bambara, R.A. (2013) Flap endonuclease 1. *Annu. Rev. Biochem.*, **82**, 119–138.
- Zheng, L., Zhou, M., Chai, Q., Parrish, J., Xue, D., Patrick, S.M., Turchi, J.J., Yannoni, S.M., Chen, D. and Shen, B. (2005) Novel function of the flap endonuclease 1 complex in processing stalled DNA replication forks. *EMBO Rep.*, **6**, 83–89.
- Li, X., Li, J., Harrington, J., Lieber, M.R. and Burgers, P.M. (1995) Lagging strand DNA synthesis at the eukaryotic replication fork involves binding and stimulation of FEN-1 by proliferating cell nuclear antigen. *J. Biol. Chem.*, **270**, 22109–22112.
- Zaher, M.S., Rashid, F., Song, B., Joudeh, L.I., Sobhy, M.A., Tehseen, M., Hingorani, M.M. and Hamdan, S.M. (2018) Missed cleavage opportunities by FEN1 lead to Okazaki fragment maturation via the long-flap pathway. *Nucleic Acids Res.*, **46**, 2956–2974.
- Sun, H., He, L., Wu, H., Pan, F., Wu, X., Zhao, J., Hu, Z., Sekhar, C., Li, H., Zheng, L. *et al.* (2017) The FEN1 L209P mutation interferes with long-patch base excision repair and induces cellular transformation. *Oncogene*, **36**, 194–207.
- Saharia, A., Teasley, D.C., Duxin, J.P., Dao, B., Chiappinelli, K.B. and Stewart, S.A. (2010) FEN1 ensures telomere stability by facilitating replication fork re-initiation. *J. Biol. Chem.*, **285**, 27057–27066.
- Teasley, D.C., Parajuli, S., Nguyen, M., Moore, H.R., Alspach, E., Lock, Y.J., Honaker, Y., Saharia, A., Pivnicka-Worms, H. and Stewart, S.A. (2015) Flap endonuclease 1 limits telomere fragility on the leading strand. *J. Biol. Chem.*, **290**, 15133–15145.
- Singh, P., Zheng, L., Chavez, V., Qiu, J. and Shen, B. (2007) Concerted action of exonuclease and Gap-dependent endonuclease activities of FEN-1 contributes to the resolution of triplet repeat sequences (CTG)<sub>n</sub>- and (GAA)<sub>n</sub>-derived secondary structures formed during maturation of Okazaki fragments. *J. Biol. Chem.*, **282**, 3465–3477.
- Guo, Z., Qian, L., Liu, R., Dai, H., Zhou, M., Zheng, L. and Shen, B. (2008) Nucleolar localization and dynamic roles of flap endonuclease 1 in ribosomal DNA replication and damage repair. *Mol. Cell Biol.*, **28**, 4310–4319.
- Tsutakawa, S.E., Thompson, M.J., Arvai, A.S., Neil, A.J., Shaw, S.J., Algaier, S.I., Kim, J.C., Finger, L.D., Jardine, E., Gotham, V.J.B. *et al.* (2017) Phosphate steering by Flap Endonuclease 1 promotes 5'-flap specificity and incision to prevent genome instability. *Nat. Commun.*, **8**, 15855.
- Bruning, J.B. and Shamoo, Y. (2004) Structural and thermodynamic analysis of human PCNA with peptides derived from DNA polymerase-delta p66 subunit and flap endonuclease-1. *Structure*, **12**, 2209–2219.
- Sakurai, S., Kitano, K., Yamaguchi, H., Hamada, K., Okada, K., Fukuda, K., Uchida, M., Ohtsuka, E., Morioka, H. and Hakoshima, T. (2005) Structural basis for recruitment of human flap endonuclease 1 to PCNA. *EMBO J.*, **24**, 683–693.
- Sharma, S., Otterlei, M., Sommers, J.A., Driscoll, H.C., Dianov, G.L., Kao, H.I., Bambara, R.A. and Brosh, R.M. Jr (2004) WRN helicase and FEN-1 form a complex upon replication arrest and together process branchmigrating DNA structures associated with the replication fork. *Mol. Biol. Cell*, **15**, 734–750.
- Sharma, S., Sommers, J.A., Gary, R.K., Friedrich-Heineken, E., Hubscher, U. and Brosh, R.M. Jr (2005) The interaction site of Flap Endonuclease-1 with WRN helicase suggests a coordination of WRN and PCNA. *Nucleic Acids Res.*, **33**, 6769–6781.
- Wang, W., Brandt, P., Rossi, M.L., Lindsey-Boltz, L., Podust, V., Fanning, E., Sancar, A. and Nigam, R.A. (2004) The human Rad9-Rad1-Hus1 checkpoint complex stimulates flap endonuclease 1. *Proc. Natl. Acad. Sci. U.S.A.*, **101**, 16762–16767.
- Querol-Audi, J., Yan, C., Xu, X., Tsutakawa, S.E., Tsai, M.S., Tainer, J.A., Cooper, P.K., Nogales, E. and Ivanov, I. (2012) Repair complexes of FEN1 endonuclease, DNA, and Rad9-Hus1-Rad1 are distinguished from their PCNA counterparts by functionally important stability. *Proc. Natl. Acad. Sci. U.S.A.*, **109**, 8528–8533.
- Cheng, I.C., Chen, B.C., Shuai, H.H., Chien, F.C., Chen, P. and Hsieh, T.S. (2016) Wuho is a new member in maintaining genome stability through its interaction with flap endonuclease 1. *PLoS Biol.*, **14**, e1002349.
- Brosh, R.M. Jr, von Kobbe, C., Sommers, J.A., Karmakar, P., Opreko, P.L., Piotrowski, J., Dianov, I., Dianov, G.L. and Bohr, V.A. (2001) Werner syndrome protein interacts with human flap endonuclease 1 and stimulates its cleavage activity. *EMBO J.*, **20**, 5791–5801.
- Friedrich-Heineken, E., Touille, M., Tannler, B., Burki, C., Ferrari, E., Hottiger, M.O. and Hubscher, U. (2005) The two DNA clamps Rad9/Rad1/Hus1 complex and proliferating cell nuclear antigen differentially regulate flap endonuclease 1 activity. *J. Mol. Biol.*, **353**, 980–989.
- Henneke, G., Koundrioukoff, S. and Hubscher, U. (2003) Phosphorylation of human Fen1 by cyclin-dependent kinase modulates its role in replication fork regulation. *Oncogene*, **22**, 4301–4313.
- Guo, Z., Zheng, L., Xu, H., Dai, H., Zhou, M., Pascua, M.R., Chen, Q.M. and Shen, B. (2010) Methylation of FEN1 suppresses nearby phosphorylation and facilitates PCNA binding. *Nat. Chem. Biol.*, **6**, 766–773.
- Hasan, S., Stucki, M., Hassa, P.O., Imhof, R., Gehrig, P., Hunziker, P., Hubscher, U. and Hottiger, M.O. (2001) Regulation of human flap endonuclease-1 activity by acetylation through the transcriptional coactivator p300. *Mol. Cell*, **7**, 1221–1231.
- Balakrishnan, L., Stewart, J., Polaczek, P., Campbell, J.L. and Bambara, R.A. (2010) Acetylation of Dna2 endonuclease/helicase and flap endonuclease 1 by p300 promotes DNA stability by creating long flap intermediates. *J. Biol. Chem.*, **285**, 4398–4404.
- Guo, Z., Kanjanapangka, J., Liu, N., Liu, S., Liu, C., Wu, Z., Wang, Y., Loh, T., Kowolik, C., Jansen, J. *et al.* (2012) Sequential posttranslational modifications program FEN1 degradation during cell-cycle progression. *Mol. Cell*, **47**, 444–456.
- Xu, H., Chen, X., Xu, X., Shi, R., Suo, S., Cheng, K., Zheng, Z., Wang, M., Wang, L., Zhao, Y. *et al.* (2016) Lysine acetylation and succinylation in HeLa cells and their essential roles in response to UV-induced stress. *Sci. Rep.*, **6**, 30212.
- Hosfield, D.J., Mol, C.D., Shen, B. and Tainer, J.A. (1998) Structure of the DNA repair and replication endonuclease and exonuclease FEN-1: coupling DNA and PCNA binding to FEN-1 activity. *Cell*, **95**, 135–146.
- Chapados, B.R., Hosfield, D.J., Han, S., Qiu, J., Yelent, B., Shen, B. and Tainer, J.A. (2004) Structural basis for FEN-1 substrate specificity and PCNA-mediated activation in DNA replication and repair. *Cell*, **116**, 39–50.
- Finger, L.D., Blanchard, M.S., Theimer, C.A., Sengerova, B., Singh, P., Chavez, V., Liu, F., Grasby, J.A. and Shen, B. (2009) The 3'-flap pocket of human flap endonuclease 1 is critical for substrate binding and catalysis. *J. Biol. Chem.*, **284**, 22184–22194.
- Tsutakawa, S.E., Classen, S., Chapados, B.R., Arvai, A.S., Finger, L.D., Guenther, G., Tomlinson, C.G., Thompson, P., Sarker, A.H., Shen, B. *et al.* (2011) Human flap endonuclease structures, DNA double-base flipping, and a unified understanding of the FEN1 superfamily. *Cell*, **145**, 198–211.
- Patel, N., Atack, J.M., Finger, L.D., Exell, J.C., Thompson, P., Tsutakawa, S., Tainer, J.A., Williams, D.M. and Grasby, J.A. (2012) Flap endonucleases pass 5'-flaps through a flexible arch using a disorder-thread-order mechanism to confer specificity for free 5'-ends. *Nucleic Acids Res.*, **40**, 4507–4519.
- Finger, L.D., Patel, N., Beddows, A., Ma, L., Exell, J.C., Jardine, E., Jones, A.C. and Grasby, J.A. (2013) Observation of unpaired substrate DNA in the flap endonuclease-1 active site. *Nucleic Acids Res.*, **41**, 9839–9847.
- Algaier, S.I., Exell, J.C., Bennet, I.A., Thompson, M.J., Gotham, V.J., Shaw, S.J., Craggs, T.D., Finger, L.D. and Grasby, J.A. (2016) DNA and protein requirements for substrate conformational changes necessary for human flap Endonuclease-1-catalyzed reaction. *J. Biol. Chem.*, **291**, 8258–8268.
- Cheng, K., Xu, H., Chen, X., Wang, L., Tian, B., Zhao, Y. and Hua, Y. (2016) Structural basis for DNA 5'-end resection by RecJ. *Elife*, **5**, e14294.
- Zhao, Y., Lu, M., Zhang, H., Hu, J., Zhou, C., Xu, Q., Ul Hussain Shah, A.M., Xu, H., Wang, L. and Hua, Y. (2015) Structural insights

- into catalysis and dimerization enhanced exonuclease activity of RNase J. *Nucleic Acids Res.*, **43**, 5550–5559.
36. Kabsch, W. (2010) Xds. *Acta Crystallogr. D Biol. Crystallogr.*, **66**, 125–132.
  37. Adams, P.D., Afonine, P.V., Bunkoczi, G., Chen, V.B., Davis, I.W., Echols, N., Headd, J.J., Hung, L.W., Kapral, G.J., Grosse-Kunstleve, R.W. *et al.* (2010) PHENIX: a comprehensive Python-based system for macromolecular structure solution. *Acta Crystallogr. D Biol. Crystallogr.*, **66**, 213–221.
  38. Emsley, P., Lohkamp, B., Scott, W.G. and Cowtan, K. (2010) Features and development of Coot. *Acta Crystallogr. D Biol. Crystallogr.*, **66**, 486–501.
  39. Zhao, Y., Gregory, M.T., Biertumpfel, C., Hua, Y.J., Hanaoka, F. and Yang, W. (2013) Mechanism of somatic hypermutation at the WA motif by human DNA polymerase eta. *Proc. Natl. Acad. Sci. U.S.A.*, **110**, 8146–8151.
  40. Shen, B., Nolan, J.P., Sklar, L.A. and Park, M.S. (1996) Essential amino acids for substrate binding and catalysis of human flap endonuclease 1. *J. Biol. Chem.*, **271**, 9173–9176.
  41. Huq, M.D., Tsai, N.P., Khan, S.A. and Wei, L.N. (2007) Lysine trimethylation of retinoic acid receptor-alpha: a novel means to regulate receptor function. *Mol. Cell Proteomics*, **6**, 677–688.
  42. Mostaqul Huq, M.D., Gupta, P., Tsai, N.P., White, R., Parker, M.G. and Wei, L.N. (2006) Suppression of receptor interacting protein 140 repressive activity by protein arginine methylation. *EMBO J.*, **25**, 5094–5104.
  43. Zheng, L., Dai, H., Zhou, M., Li, M., Singh, P., Qiu, J., Tsark, W., Huang, Q., Kernstine, K., Zhang, X. *et al.* (2007) Fen1 mutations result in autoimmunity, chronic inflammation and cancers. *Nat. Med.*, **13**, 812–819.
  44. Exell, J.C., Thompson, M.J., Finger, L.D., Shaw, S.J., Debreczeni, J., Ward, T.A., McWhirter, C., Sioberg, C.L., Martinez Molina, D., Abbott, W.M. *et al.* (2016) Cellularly active N-hydroxyurea FEN1 inhibitors block substrate entry to the active site. *Nat. Chem. Biol.*, **12**, 815–821.
  45. Tsutakawa, S.E., Lafrance-Vanasse, J. and Tainer, J.A. (2014) The cutting edges in DNA repair, licensing, and fidelity: DNA and RNA repair nucleases sculpt DNA to measure twice, cut once. *DNA Repair (Amst.)*, **19**, 95–107.
  46. AlMalki, F.A., Flemming, C.S., Zhang, J., Feng, M., Sedelnikova, S.E., Ceska, T., Rafferty, J.B., Sayers, J.R. and Artymiuk, P.J. (2016) Direct observation of DNA threading in flap endonuclease complexes. *Nat. Struct. Mol. Biol.*, **23**, 640–646.
  47. Bedford, M.T. and Clarke, S.G. (2009) Protein arginine methylation in mammals: who, what, and why. *Mol. Cell*, **33**, 1–13.
  48. Flanagan, J.F., Mi, L.Z., Chruszcz, M., Cymborowski, M., Clines, K.L., Kim, Y., Minor, W., Rastinejad, F. and Khorasanizadeh, S. (2005) Double chromodomains cooperate to recognize the methylated histone H3 tail. *Nature*, **438**, 1181–1185.
  49. Hughes, R.M. and Waters, M.L. (2006) Arginine methylation in a beta-hairpin peptide: implications for Arg-pi interactions, DeltaCp(o), and the cold denatured state. *J. Am. Chem. Soc.*, **128**, 12735–12742.
  50. Li, S., Ali, S., Duan, X., Liu, S., Du, J., Liu, C., Dai, H., Zhou, M., Zhou, L., Yang, L. *et al.* (2018) JMJD1B demethylates H4R3me2s and H3K9me2 to facilitate gene expression for development of hematopoietic stem and progenitor cells. *Cell Rep.*, **23**, 389–403.